Micro-continuum modeling of biofilm growth coupled with hydrodynamics in OpenFOAM

Romain Guibert, Pierre Horgue, Gerald Debenest

SoftwareX 29 (2025) 102011

Contents lists available at ScienceDirect

SoftwareX

journal homepage: www.elsevier.com/locate/softx

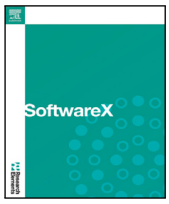

Original software publication

Micro-continuum modeling of biofilm growth coupled with hydrodynamics in OpenFOAM

Romain Guibert *, Pierre Horgue, Gérald Debenest

Institut de Mécanique des Fluides de Toulouse (IMFT) - Université de Toulouse, CNRS-INPT-UPS, Toulouse, France

ARTICLE INFO

Keywords:
Biofilm
Computational fluid dynamics
Porous media
Bio-clogging
OpenFOAM

ABSTRACT

Biofilm growth is a complex phenomenon that couples species transport and reactions with fluid flow dynamics. Simulating these processes in complex geometries remains challenging due to the different time and space scales, as well as the associated computational cost. `biofilmFoam` is a toolbox based on OpenFOAM that couples advection–diffusion equations with source terms (related to the reactions involved) with the dynamics of the surrounding fluid. This framework provides an efficient basis for performing reliable simulations on any domain or for building more complex models.

Code metadata

Current code version	v2409
Permanent link to code/repository used for this code version	https://github.com/ElsevierSoftwareX/SOFTX-D-24-00468
Permanent link to Reproducible Capsule	
Legal Code License	GNU GPL V3
Code versioning system used	git
C++	
Compilation requirements, operating environments & dependencies	OpenFOAM v2206 and following versions
If available Link to developer documentation/manual	https://biofilmfoam.readthedocs.io
Support email for questions	romain.guibert@imft.fr

1. Motivation and significance

Biofilms represent a significant portion of microbial life and have been extensively studied for over a century, both in the laboratory and in their natural environment. However, there are still many open questions regarding their development [1], spanning from the attachment phase to the maturation and dispersion phases. Therefore, modeling biofilm growth remains a challenge, both in terms of understanding the phenomena involved and the influence of the environment. Various models have been proposed in the literature [2], which can be classified into two main categories, continuum and discrete approaches.

These approaches differ significantly in their overall conceptual framework. Continuum models are based on the population-averaged behavior of microorganisms, treating biomass as a whole and describing its evolution with partial differential equations. In contrast, discrete models focus on the actions and interactions between individual subunits, from which the biofilm's evolution emerges, employing methods such as cellular automata or agent-based models.

Continuum models are often used to describe the macroscopic behavior of biofilms [3], such as their growth kinetics or their response to environmental changes [3–6]. They are well suited for simulating large-scale systems. On the other hand, discrete models (based on cellular automaton models or individual-based models) allow for a more detailed description of biofilm structure and dynamics. They can account for the variability of microbial behavior, and the influence of local environmental conditions on biofilm development [7–10]. However, they may require more experimental data for calibration and validation. Hybrid approaches have also been proposed, combining continuum and discrete models to take advantage of their respective strengths [11,12].

* Corresponding author.
E-mail address: romain.guibert@imft.fr (Romain Guibert).

https://doi.org/10.1016/j.softx.2024.102011
Received 4 September 2024; Received in revised form 6 December 2024; Accepted 8 December 2024
Available online 26 December 2024

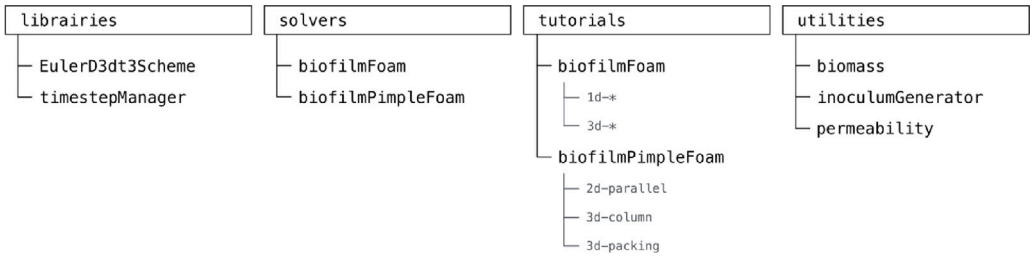

Fig. 1. Architecture of the `biofilmFoam` package.

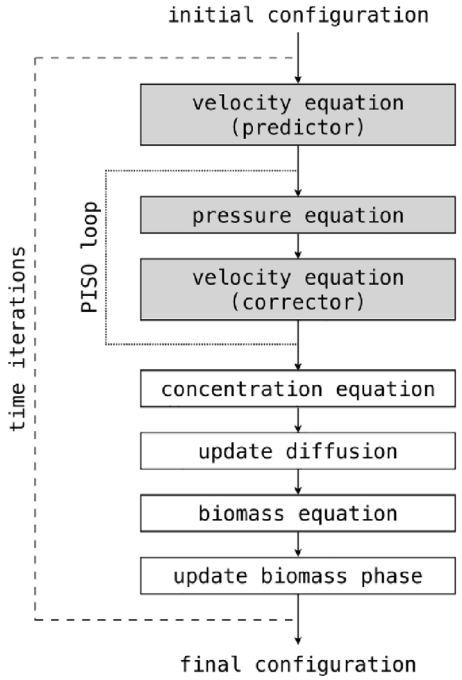

Fig. 2. Schematic of the sequential algorithms. The gray boxes are only present in the `biofilmPimpleFoam` solver, coupling biofilm spreading and hydrodynamics.

Creating a single biofilm model that accurately represents all possible evolution scenarios and complex interactions with micro-environments is challenging. However, developing a unified environment that resolves fluid flow coupled with biofilm development is intriguing. We opted for a continuum growth model which allows a relatively straightforward coupling with fluid dynamics, also solved using a continuous model.

2. Software description

2.1. Mathematical model

The original model proposed by [4] distinguishes between fluid Ω_f domain and biofilm domain Ω_b ($\Omega = \Omega_f \cup \Omega_b$). The density-diffusion modeling of biofilm growth is defined as

$$\frac{\partial c}{\partial t} + \mathbf{u}\cdot\nabla c = \nabla\cdot\left(d_1(m)\nabla c\right) - f(c,m) \tag{1}$$

$$\frac{\partial m}{\partial t} = \nabla\cdot\left(d_2(m)\nabla m\right) + g(c,m) \tag{2}$$

where $c(t,\mathbf{x})$ is the nutrient concentration, $m(t,\mathbf{x})$ is the biomass density, $\mathbf{u}$ is the fluid velocity, $d_i(m)$ (with $i = 1,2$) are diffusion coefficients, $f(c,m)$ is the nutrient consumption rate and $g(c,m)$ is the biomass production rate. Eq. (1) describes the transport and consumption of nutrients, with a diffusive coefficient that varies with biomass content. Note that only diffusion occurs in the biofilm phase, as there is no flow. Eq. (2) describes the evolution of biomass density and the production term $g(c,m)$ also contains a wastage term. The definitions of consumption rate, production rate, and diffusion coefficients are reported in Appendix A. All the numerical values used for the biofilm model parameters are reported in Appendix B.

In addition, the flow modeling of the surrounding hydrodynamics is performed using a Darcy–Brinkman approach [13], following

$$\frac{1}{\phi}\left(\frac{\partial \rho\mathbf{u}}{\partial t} + \nabla\cdot\left(\frac{\rho}{\phi}\mathbf{u}\mathbf{u}\right)\right) = -\nabla p + \frac{\mu}{\phi}\nabla^2\mathbf{u} - \frac{\mu}{k}\mathbf{u} \tag{3}$$

$$\nabla\cdot\mathbf{u} = 0 \tag{4}$$

where ϕ is the porosity, ρ is the fluid density, p is the pressure field, μ is the dynamic viscosity of fluid and k is the permeability. Due to the Darcy drag term in Eq. (3), the Navier–Stokes equations tend to Darcy equation in the biofilm phase, where is defined the permeability. One of the main challenges in numerically solving the system of Eqs. (1)–(4) is the significant disparity in time scales between the rapid changes in flow structure and the slow growth of biomass.

The classical CFD approach uses a Courant number to ensure the stability of the Navier–Stokes equations. However, this method results in very small time steps relative to the simulation times needed to observe biomass evolution, making the simulations prohibitively expensive.

However, if we consider a pre-established flow within a given geometry with stationary boundary conditions, changes in velocity and pressure fields are solely related to biomass growth. Under these conditions, it is possible to set up a time step management system based on time truncation error estimates applied to the biofilm variables, c and m, similar to what is done in [14]. It is important to note that the stability and reliability of simulations performed with abrupt variations in flow properties, independent of biofilm evolution such as pump stop for example, are not guaranteed with this approach. In this case, assuming a separation of time scales between flow and biofilm, it is possible to calculate the new hydrodynamic steady state before modeling the biofilm growth.

2.2. Software architecture

The source code supplied has the classic structure of OpenFOAM tools, as shown in Fig. 1. The `biofilmFoam` solver only simulates biofilm spreading, as in [4], while the `biofilmPimpleFoam` solver takes hydrodynamic coupling into account. For each solver, several illustrative cases are provided in `tutorials` folder, and initialization and post-processing tools are also available in `utilities`. The online code documentation provides details on several tutorials, along with utilities and their respective functions.

2.3. Numerical methods

The provided solvers are standard in the OpenFOAM environment. The equations are solved sequentially as shown in Fig. 2. Time step management based on truncation error is available for three time schemes in OpenFOAM: *Euler*, *backward*, and *CrankNicolson*.

In the illustrative cases proposed in the following, a classical second-order centered scheme is used for spatial discretization and a second-order *backward* scheme is used for time discretization.

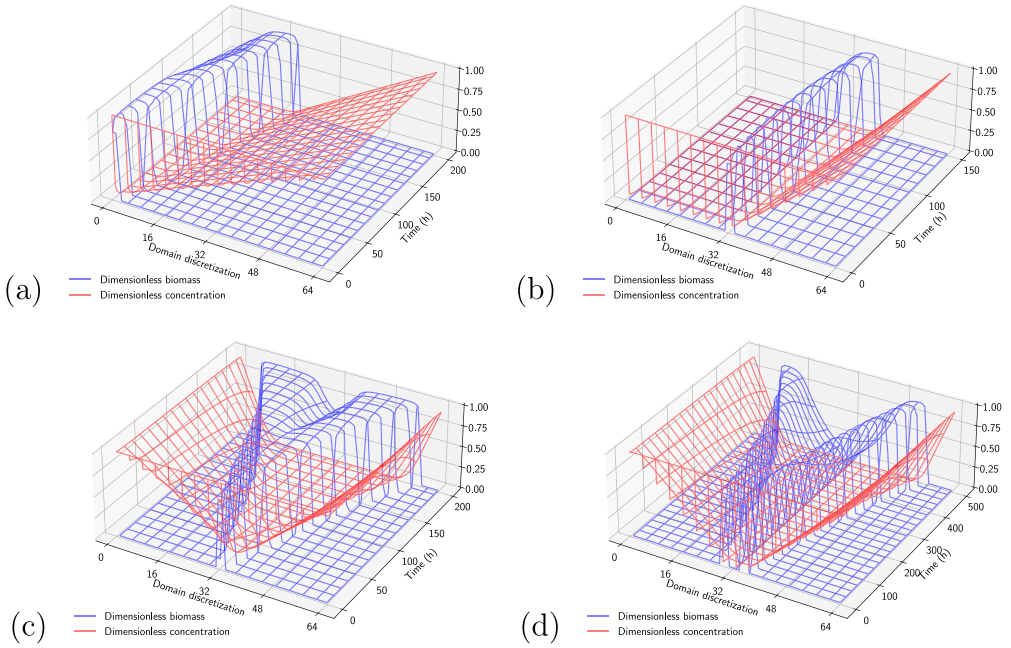

Fig. 3. Temporal evolutions of dimensionless nutrient concentration C and dimensionless biomass M for different one-dimensional configurations: (a) biofilm growth on a surface, (b) biofilm growth under non-symmetric conditions, (c) biofilm growth under symmetric conditions and (d) merging of colonies.

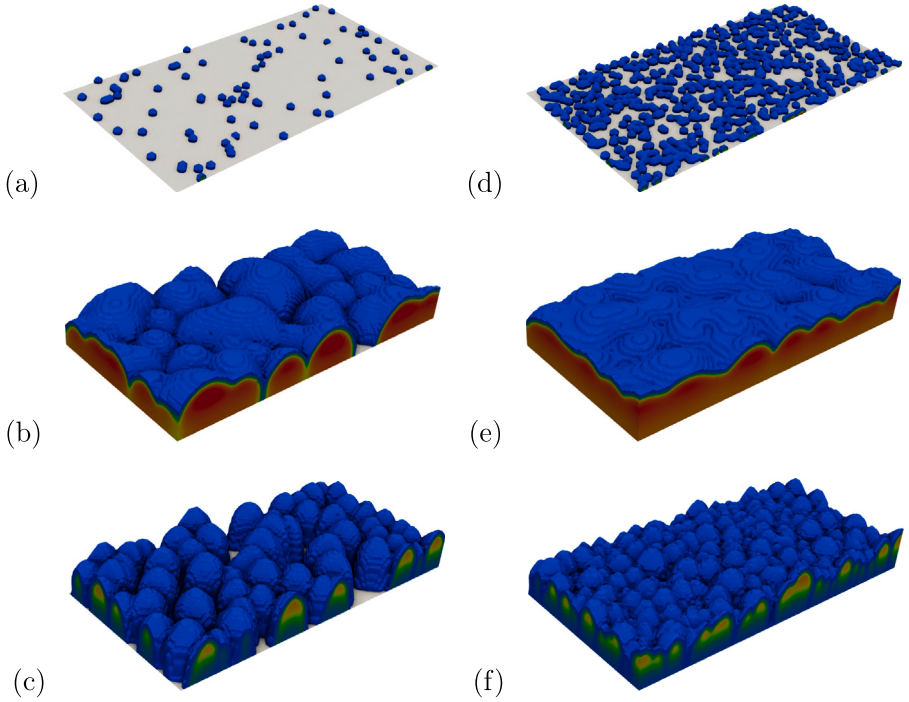

Fig. 4. Biofilm phase configurations. (left) 1% and (right) 10% of the lower side is inoculated. Two sets of parameters are used for inoculation: (b, e) high concentration and low maximum biomass and (c, f) low concentration and high maximum biomass. These illustrations correspond to different physical times, when 30% of the domain height has been reached.

3. Illustrative examples

3.1. Biofilm growth

One-dimensional cases

This first set of validation cases corresponds to the illustrative one-dimensional cases proposed in [4]. In these configurations, various simple situations without flow are tested. The domain consists of 64 cells (with a cell size of 1.6 μm), with one or more blocks of two cells being inoculated. The adaptive time step is limited by a truncation error of 1 ‰. The results are illustrated in Fig. 3.

For configuration 3a, the initial inoculum is located at the left end of the domain, i.e. on a surface, and the nutrient is supplied by pure diffusion from the right end of the domain. In configuration 3b, the inoculum is placed at the center of the domain, and nutrients are supplied exclusively from the right-hand side. Configuration 3c is identical to the previous one, except that the nutrient supply is symmetrical, coming from both sides of the domain. Finally, configuration 3d illustrates the temporal evolution of two close but disjoint inoculum under symmetrical nutrient supply.

The results obtained are fully comparable to the initial results [4], although the numerical methods used are different.

Biofilm types

Still neglecting coupling with hydrodynamics, and as observed by [4], we can evaluate the model's ability to produce different types of biofilm. For the cases illustrated in this section, the domain is formed of $128 \times 64 \times 64$ cells (with a cell size of 1.89 μm). Nutrients are supplied by the upper surface of the domain (by pure diffusion) and different portions of the lower surface are inoculated (approx. 1% and 10%). Inoculation is performed randomly (using `inoculumGenerator`), by depositing several spots of biomass, each within a single computational cell. Simulations are conducted until the biofilm phase reaches 30% of the domain height the time step is limited to ensure a 1% truncation error.

Fig. 4 reports two distinct biofilm types obtained by modifying the model's parameters, i.e. maximum biomass and nutrient concentration.

As observed in [4], when nutrients are limited (Figs. 4c, 4f), colonies propagate horizontally with much greater difficulty, and colonies hardly merge. On these hydrostatic configurations, we observe biofilm growth patterns very similar to the original implementation, representing a good basis for coupling with hydrodynamics.

3.2. Coupling with hydrodynamics

Two-dimensional configuration

To start with a relatively simple coupling case, we study the growth of a biofilm between two surfaces (separated by a distance h). The domain is formed of 512×64 cells, with a cell size of 1.89 μm (as for all 3D cases, in accordance with [4]). Both surfaces are inoculated in equal proportions, nutrient concentration arrives from the left, and growth is observed for different Reynolds numbers (here $Re = \rho U_{\text{in,max}} h/\mu$). Fig. 5 shows the biofilm growth patterns after 4 days for different numbers of Reynolds from 0.1 to 1, as macroscopic evaluations of biomass volumes and permeabilities.

These simulations are carried out with the same inoculation configuration. We observe that for $Re < 1$, the nutrient supply by the fluid is not sufficient to allow uniform growth along the length and colonies close to the inlet grow fastest. On the seven days of simulations realized, only configurations with $Re > 1$ end up clogging the domain.

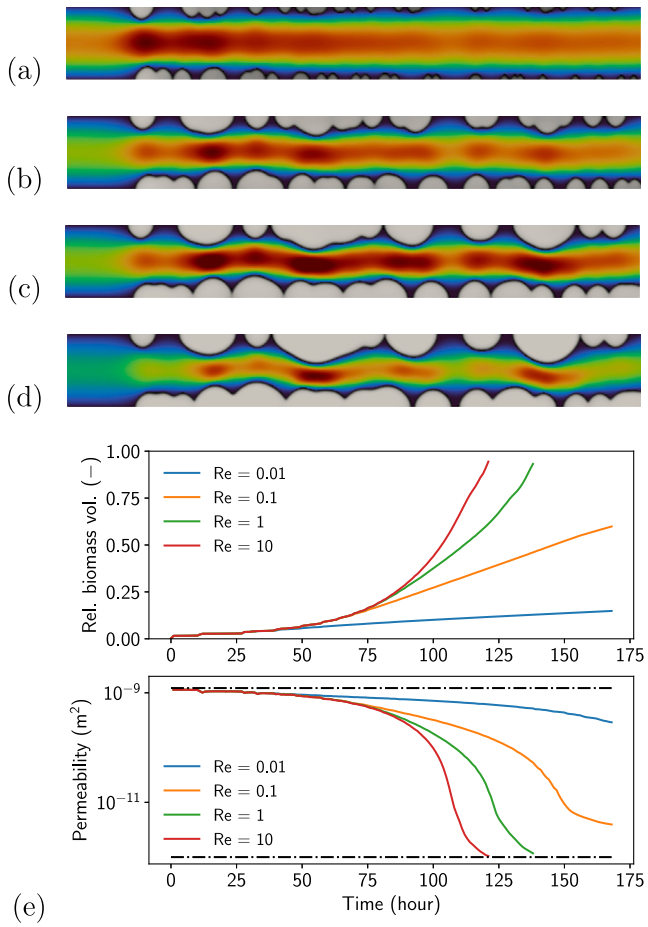

Fig. 5. (a–d) Illustrations of biofilm growth after four days for the same inoculated surface (close to 5%): (a) $Re = 0.01$, (b) $Re = 0.1$, (c) $Re = 1$ and (d) $Re = 10$. (e) Evolution of biomass and permeability. Dash-dotted lines represent permeability without the biofilm phase (high) and permeability imposed in the phase (low).

Spheres configurations

In this configuration, a 200 μm diameter cylinder is filled with a vertical array of spheres (20% smaller in diameter than the cylinder). The flow is from the top surface, where the nutrient is at its higher concentration. The two central spheres are contaminated (1% of their surface). The figure shows the evolution of the biofilm development in two flow regimes, after 2 and 5 days.

For 3D configurations, the Reynolds number is defined as $Re = \rho q d/\mu A \epsilon$, where q is the flow rate, d is the grain diameter, A is the cross-sectional area and ϵ is the porosity. At shorter times, as shown in Figs. 6a, 6c the biofilm evolutions are relatively similar, but this is no longer the case at longer times. As shown in the two-dimensional case above, after five days, when the flow is low (here $Re = 0.01$), the nutrient promotes biofilm growth on the first sphere (Fig. 6b). At higher flow rates ($Re = 1$), growth is uniform on both spheres (Fig. 6d).

Spheres packing

This case is built from an open-source packing of equal hard spheres [15]. A cylinder with a height of 500 voxels and a diameter of 100 voxels is extracted from the provided 3D image. Spheres are 50 voxels in diameter. As before, the flow comes from the top surface, and the inoculum is distributed over the surface of the spheres over 80% of the total height.

As shown in Fig. 7, the biofilm grows steadily from the inoculated regions, and by day six, the upper part of the medium is completely clogged. These observations are comparable to those obtained experimentally [5,16,17].

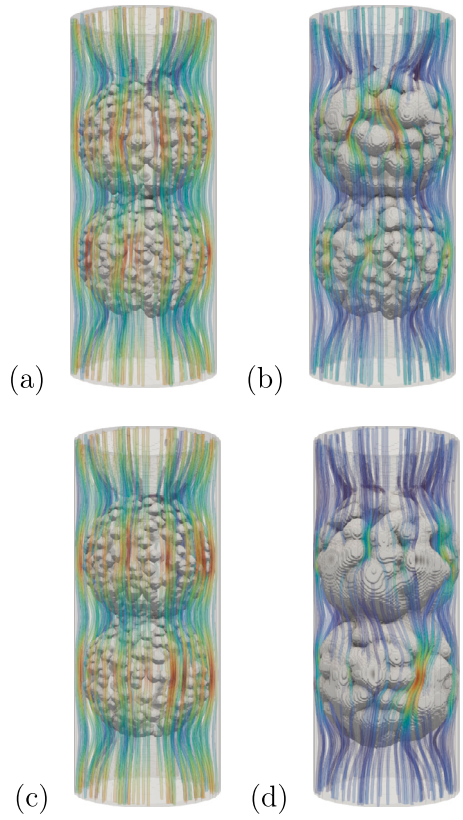

Fig. 6. Illustration of biofilm spreading on a sphere alignment for two flow regimes: (a, b) $Re = 0.01$ and (c, d) $Re = 1$. Instantaneous configurations after (a, c) 2 days and (b, d) 5 days.

For this configuration, the mesh consists of 1.3 million cells. We use 2nd-order spatial and temporal discretization schemes, and the time step is driven by a 1% truncation error. For reference, the computation time on a desktop machine, with an Intel®Xeon®Gold 6430 processor (32 physical cores), is just over 5 h CPU (579s physical) for the 6 physical days.

4. Impacts and conclusions

We have developed an open-source toolbox dedicated to the simulation of biofilm growth coupled with the surrounding hydrodynamics within the OpenFOAM framework. Currently, there is one available biofilm model [4] implemented, and our implementation reproduces the behavior observed in the original work. The presented cases of coupling with hydrodynamics are primarily illustrative of the capabilities of the tool and should be directly calibrated against experiments.

This tool is designed for both experienced OpenFOAM users, who can easily use the tool and adapt it to their needs, and for novice OpenFOAM users, who can refer to the associated documentation.

The novelty of the toolbox lies in its ability to couple biofilm growth with the surrounding fluid dynamics, all within a single tool that offers interesting parallel efficiency. This aspect makes it possible to investigate bio-clogging phenomena, for example, in complex heterogeneous media [5,16,17]. Another possible further development of the tool is related the complexity of the growth modeling. It is possible to implement other models, taking advantage of existing ones to start developments, and to look at more complex configurations with for example several species [18], or in the presence of limiting factors [19], or based on different physics [5].

CRediT authorship contribution statement

Romain Guibert: Writing – review & editing, Writing – original draft, Visualization, Validation, Software, Methodology, Investigation, Conceptualization. **Pierre Horgue:** Writing – review & editing, Methodology. **Gérald Debenest:** Writing – review & editing, Supervision.

Declaration of competing interest

The authors declare that they have no known competing financial interests or personal relationships that could have appeared to influence the work reported in this paper.

Appendix A. Details of biofilm model

In this appendix, we provide details on the diffusion coefficients $d_i(m)$, the nutrient consumption rate $f(c,m)$ and the biomass production rate $g(c,m)$ that appear in the biofilm growth model (1)–(2).

Whereas the diffusion coefficient d_1 appearing in the concentration Eq. (1) is constant, the density-dependent diffusion coefficient, related to biomass Eq. (2), is defined by

$$d_2(m) = \left(\frac{\epsilon}{m_{max} - m}\right)^a m^b \tag{A.1}$$

with ϵ, a and b non-dimensional parameters, and m_{max} the maximal biomass density.

The nutrient consumption rate $f(c,m)$ and the biomass production rate $g(c,m)$ are defined by

$$f(c,m) = \frac{k_1 cm}{k_2 + c} \tag{A.2}$$

$$g(c,m) = k_3(f(c,m) - k_4\ m) \tag{A.3}$$

where the parameters k_i (with $i = 1,\dots,4$) are expressed as

$$k_1 = \frac{\mu_m}{Y_{XS}} + m_s \tag{A.4}$$

with μ_m the specific growth rate, Y_{XS} the substrate growth yield factor and m_s the maintenance coefficient,

$$k_2 = K_s \tag{A.5}$$

with K_s the Monod saturation constant,

$$k_3 = \frac{Y_{XS}}{m_{max}} \tag{A.6}$$

and

$$k_4 = m_s m_{max} \tag{A.7}$$

The biofilm model version implemented in the supplied code is a dimensionless version, based on the dimensionless variables $M = m/m_{max}$ and $C = c/c_0$, with c_0 the maximal nutrient concentration. The numerical values of the different parameters are synthesized in Appendix B.

Appendix B. Numerical values

This appendix reports the numerical values used for the various parameters of the biofilm model. Many of these parameters are constant for all the cases studied. For the others, we give the range of values used. All the numerical values used are reported in Table B.2.

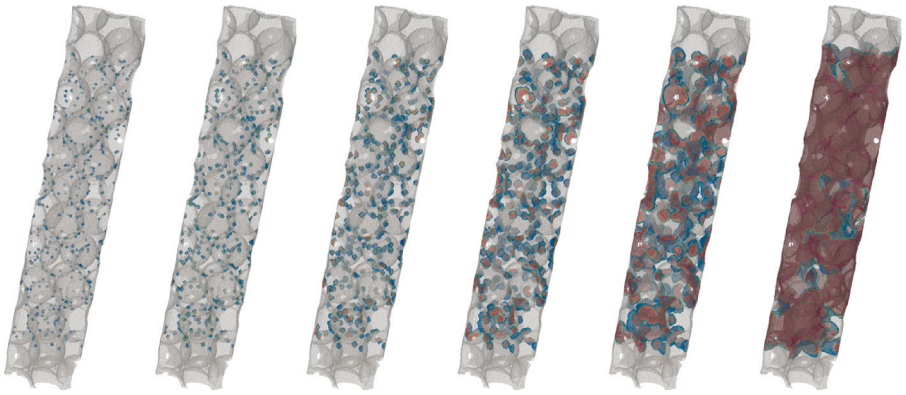

Fig. 7. Evolution of the biofilm growth in spheres packing, at $Re = 1$ and for a random initial inoculation on 1‰ of the solid surface. From left to right, snapshots every 24 h, from one to six days.

Table B.2
Numerical values for biofilm model parameters.

Parameter	Unit	Value
d_1	m/s	1.6×10^{-9}
μ_m	s^{-1}	1.5×10^{-5}
Y_{XS}	–	0.045
K_s	kg/m^3	$[1.5, 3.5] \times 10^{-5}$
m_s	s^{-1}	3×10^{-5}
m_{max}	kg/m^3	$[30, 90]$
c_0	kg/m^3	$[0.6, 4] \times 10^{-3}$
M_0	–	0.8
ϵ	–	$[0.1, 1] \times 10^{-4}$
a	–	4
b	–	4

References

[1] Sauer K, Stoodley P, Goeres DM, Hall-Stoodley L, Burmø lle M, Stewart PS, Bjarnsholt T. The biofilm life cycle: Expanding the conceptual model of biofilm formation. Nat Rev Microbiol 2022;20(10):608–20.

[2] Mattei M, Frunzo L, D'acunto B, Pechaud Y, Pirozzi F, Esposito G. Continuum and discrete approach in modeling biofilm development and structure: a review. J Math Biol 2018;76:945–1003.

[3] Wanner O, Gujer W. A multispecies biofilm model. Biotechnol Bioeng 1986;28(3):314–28.

[4] Eberl HJ, Parker DF, Vanloosdrecht MC. A new deterministic spatio-temporal continuum model for biofilm development. Comput Math Methods Med 2001;3(3):161–75.

[5] Peszynska M, Trykozko A, Iltis G, Schlueter S, Wildenschild D. Biofilm growth in porous media: Experiments, computational modeling at the pore scale, and upscaling. Adv Water Resour 2016;95:288–301.

[6] Emerenini BO, Hense BA, Kuttler C, Eberl HJ. A mathematical model of quorum sensing induced biofilm detachment. PLoS One 2015;10(7):e0132385.

[7] Picioreanu C, Van Loosdrecht MC, Heijnen JJ. Mathematical modeling of biofilm structure with a hybrid differential-discrete cellular automaton approach. Biotechnol Bioeng 1998;58(1):101–16.

[8] Tang Y, Valocchi AJ. An improved cellular automaton method to model multispecies biofilms. Water Res 2013;47(15):5729–42.

[9] Von Der Schulenburg DG, Pintelon T, Picioreanu C, Van Loosdrecht M, Johns M. Three-dimensional simulations of biofilm growth in porous media. AIChE J 2009;55(2):494–504.

[10] Cockx BJ, Foster T, Clegg RJ, Alden K, Arya S, Stekel DJ, Smets BF, Kreft J-U. Is it selfish to be filamentous in biofilms? Individual-based modeling links microbial growth strategies with morphology using the new and modular idynomics 2.0. PLoS Comput Biol 2024;20(2):e1011303.

[11] Laspidou CS, Rittmann BE. Modeling the development of biofilm density including active bacteria, inert biomass, and extracellular polymeric substances. Water Res 2004;38(14–15):3349–61.

[12] Boraey MA, Guaily A, Epstein M. A hybrid model for biofilm growth on a deformable substratum. Can J Chem Eng 2015;93(5):789–97.

[13] Soulaine C, Roman S, Kovscek A, Tchelepi HA. Mineral dissolution and wormholing from a pore-scale perspective. J Fluid Mech 2017;827:457–83.

[14] Horgue P, Renard F, Gerlero GS, Guibert R, Debenest G. PorousMultiphaseFoam v2107: An open-source tool for modeling saturated/unsaturated water flows and solute transfers at watershed scale. Comput Phys Comm 2022;273:108278.

[15] Finney J. Finney packing of spheres. 2016, http://dx.doi.org/10.17612/P78G69, https://www.digitalrocksportal.org/projects/47.

[16] Davit Y, Iltis G, Debenest G, Veran-Tissoires S, Wildenschild D, Gérino M, Quintard M. Imaging biofilm in porous media using x-ray computed microtomography. J Microsc 2011;242(1):15–25.

[17] Ostvar S, Iltis G, Davit Y, Schlüter S, Andersson L, Wood BD, Wildenschild D. Investigating the influence of flow rate on biofilm growth in three dimensions using microimaging. Adv Water Resour 2018;117:1–13.

[18] Eberl HJ, Collinson S. A modeling and simulation study of siderophore mediated antagonism in dual-species biofilms. Theor Biol Med Modell 2009;6:1–16.

[19] Ghasemi M, Eberl HJ. Time adaptive numerical solution of a highly degenerate diffusion–reaction biofilm model based on regularisation. J Sci Comput 2018;74:1060–90.